# ZERO-POWER MULTI-THRESHOLD TEMPERATURE SENSOR BASED ON SHAPE MEMORY ALLOY ANTENNA

*Wenxin Zeng, Wei Wang, and Sameer Sonkusale**
Department of Electrical and Computer Engineering, Tufts University, USA
Nano Lab, Advanced Technology Laboratory, Tufts University, USA

## ABSTRACT

Monitoring critical temperature transition events is essential for perishable goods during transportation. However, conventional sensors require expensive electronics and continuous power sources for their functioning, which makes it impractical for cost and logistical reasons for monitoring a large number of goods. Based on our previous work using shape memory alloy or SMA, we propose a zero-power multi-section SMA-wire-based antenna that can record multiple levels of critical temperature crossing events without any need for peripheral electronic components or batteries. This paper presents details of fabrication and test/validation efforts of the shape memory effect of the conjoined multi-section SMA antenna for the recording of temperature violation events.

## KEYWORDS

Antenna, temperature threshold sensor, shape memory alloy, zero-power sensors, near-zero sensors.

## INTRODUCTION

With the advent of the era of Internet-of-Things (IoT), there has been a growing need for smart sensors that are low-cost and energy-efficient. In scenarios where a large number of sensors are needed, conventional sensors that consist of electronic memory, controller units, and power supply are quite expensive to deploy at a large scale. The need for a continuous power source is a logistical bottleneck in many applications. Recently, zero-powered sensors have been investigated to address this need. This includes humidity sensors [1,2,3,4], strain sensors [5,6], and tile sensors [7,8]. Other zero-power single-event sensors such as photoswitches [9], package security sensors [10,11], liquid level sensor [12], corrosion sensor [13], and home security sensors [14,15,16] have also been reported, employing different techniques for fabrication. For communication of sensor information, passive Radio-frequency identification (RFID) tags are preferred since it does not need a battery and relies on the backscattering of signal sent by an interrogating reader [17,18].

While the aforementioned sensors may offer zero-power real-time detection, they need peripheral electronic devices to record the sensed information until it is read out by the reader. This data-logging operation is in by itself power-hungry. In some applications, a detailed recording of the whole time is unnecessary, and only some critical events are of interest to the monitoring personnel. For instance, certain goods need to be stored in a certain temperature range, such as chemicals and drugs [19]. Violation in temperature can cause degradation or even adverse effects on these products. Conventional sensors would record the whole temperature history of the goods, while in reality, one is only interested in monitoring whether the temperature threshold was ever crossed. Thus, it will be beneficial to develop a zero-power sensor that can also record those temperature events in by itself for posterity without the need for data logging memory units.

Due to its thermal-mechanical properties, shape memory alloy (SMA) can be used for recording temperature events. It has been used for reconfigurable antenna [20] and temperature sensing [21,22]. In prior work, a battery-free threshold temperature sensor was developed by utilizing the shape change of the SMA as a detector/recorder of events [23]. Relying on the shape memory effect of SMA, the antenna irreversibly changes its configuration from parallel to dipole antenna when the temperature rises above the threshold value. As a result, its radiation profile is altered. The antenna would lock this configuration even after the temperature drops back below the threshold temperature value. This sensor is used to record the temperature violation event without a memory device and power supply, but its usage is limited to monitoring a single threshold level crossing. This article proposes an SMA-based multi-threshold temperature sensor, which can monitor the goods with more detailed historical temperature information and multiple threshold temperature level crossing events. The sensor consists of two SMA sections with different temperature thresholds to provide a more complex shape reconfiguration. This can be scaled up to multiple sections for a more complex temperature monitoring profile.

## PRINCIPLE OF SENSOR OPERATION

### Properties of Shape Memory Alloy

SMAs are metals that have a memory effect depending on environmental temperature. Most SMAs are alloys made of nickel and titanium. At a low temperature, the SMA is in its martensite state. Atoms are loosely patterned in this state so that the shape of SMA can be easily modified. While at high temperature, the SMA is in the austenite state, where the atoms are tightly arranged, making the whole SMA stiff and rigid [24,25]. When the temperature rises above the threshold, heat is absorbed by the SMA, and the rearranging force between atoms makes the SMA recover to its predefined shape, regardless of its previous deformed shape, which presents the memory effect. As shown in Figure 1, the start and end temperatures for the state-changing from martensite to austenite are $A_s$ and $A_f$, respectively; the start and end temperatures for the state changing from austenite to martensite are $M_s$ and $M_f$, respectively [26,27]. Due to the hysteresis, the SMA will keep its shape in austenite form, even if the temperature drops below $A_s$ but above $M_s$.

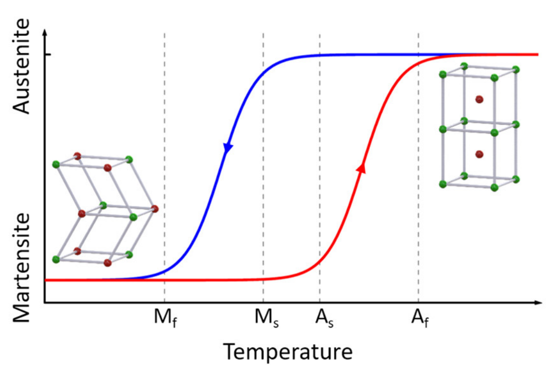


*Figure 1: The hysteresis and critical temperature threshold of shape memory alloy. Inserts are Martensite and Austenite crystal structures.*

978-1-940470-04-7/HH2022/$25©2022TRF
DOI 10.31438/trf.hh2022.99

Using this shape memory and self-recovery nature of the SMA, an SMA-based antenna is designed for wireless temperature crossing event sensing. To monitor different levels of temperature crossing events, two sections of SMA wire with varying thresholds of temperature are conjoined to form the SMA-based antenna. Each section will recover to its predefined configuration when the temperature exceeds its respective threshold, which leads to different radiation profiles for each crossing event. By sensing and differentiating this radiation information, the key historical temperature information is recorded for posterity and easily recovered.

### Sensor Design and Simulation

The sensor is designed as an antenna consisting of two arms that change shape under different temperature conditions, as in Figure 2. Each arm composes one red color section made by a low-temperature threshold SMA of threshold value $T_1$, and another blue color section fabricated with an SMA with a high-temperature threshold of $T_2$. The sensor is connected to a tiny PCB board. When the temperature is less than $T_1$, the whole sensor is in a martensite state and is manually reset to the shape shown in Figure 2(a). When the temperature rises above $T_1$ but below $T_2$, the red section recovers its predefined shape forming a straight line, which results in a dipole antenna configuration, as shown in Figure 2(b). This shape reconfiguration (Figure 2(b)) has a different radiation profile than the previous case (Figure 2(a)). Even if the temperature drops back below $T_1$, the antenna will still hold this dipole antenna configuration. Thus, the temperature crossing event at $T_1$ is recorded for posterity in the natural shape/state of the SMA antenna. When the temperature further exceeds $T_2$, which indicates the second temperature crossing event, the blue section recovers to its predefined straight shape, as shown in Figure 2(c). This causes the sensor to form a parallel line configuration. The parallel line antenna has very low radiation since the signals on the two arms cancel each other. Similarly, if the temperature drops below $T_2$, the antenna will still hold the parallel line shape, thus recording the prior temperature crossing event. By sensing and differentiating the radiation profile in its different configurations, the historical temperature information can be revealed.

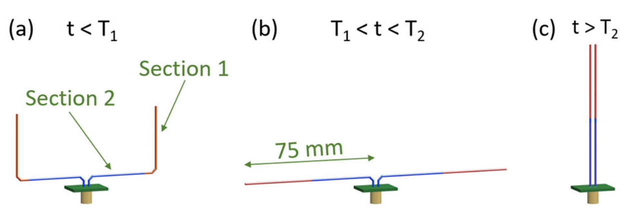


*Figure 2: SMA antennas morph into different shapes at different temperature levels. (a) Below the lower threshold, (b) Between two thresholds, and (c) above the second threshold.*

In our measurement, the shape variation caused by temperature violation is detected by the reflection coefficient $S_{11}$. When the temperature exceeds each of these thresholds, the reflection coefficient differs. To quantify the results, $S_{11}$ of the different states of the SMA antenna is simulated. The total length of each multi-section SMA wire is 75 mm, which results in a magnitude peak at 950 MHz in the range of UHF RFID. At a temperature below $T_1$, the SMA sensor is deformed in a U shape. Under this condition, the impedance of the antenna is 44+5j Ω at 950 MHz. When the temperature is between $T_1$ and $T_2$, the antenna switches to a dipole antenna configuration, and the impedance changes to 73+9j Ω. As a result, the minimal magnitude of the return loss $S_{11}$ around 950MHz decreases from 24 dB to 17 dB. When further temperature crossing occurs, the temperature rising above $T_2$, the SMA wires straighten and form a parallel line antenna. At this point, the impedance of the antenna is 1−29 j Ω. The $S_{11}$ flattens out at 0 dB over the simulated frequency range of 0.7 GHz to 1.2 GHz.

## FABRICATION AND CHARACTERIZATION

SMA wires with a diameter of 0.5 mm are used to fabricate the SMA antenna. The thresholds $T_1$ and $T_2$ of the two SMA wires are chosen as 30 °C and 50 °C, respectively. The detailed fabrication process of the SMA wire with a specific threshold can be obtained from [28].

To fabricate the multi-section SMA antenna, SMA wires need to be electrically joined together. Soldering is preferred for its robust connection. However, the ordinary soldering process would fail due to the formation of an oxide layer on the surface of the SMA wire [29]. The heat during the soldering greatly accelerates the oxidation process. To eliminate oxidation, phosphoric acid is applied to the polished ends of two SMA wires before soldering [30]. The phosphoric acid wetting on the SMA wires prevents oxidation. Therefore, the two parts can be soldered together. A physically and electrically stable connection is created between the sections of the SMA wire. Afterward, the residue of phosphoric acid and excessive solder is removed for a smooth connection. An antenna is formed by attaching the conjoined multi-section SMA wires to a tiny printed circuit board.

### Temperature Response

The temperature response of the sensor is measured by recording the shape of the SMA wire while sweeping the temperature. To ensure that the environment temperature is stable, the fabricated SMA wire is submerged in a water bath, which allows the temperature to be precisely controlled. A thermocouple (RISEPRO) is placed nearby the SMA sensor to detect the environmental temperature. The fabricated multi-section SMA wire is initially cooled at 5 °C in the water bath, and then gradually heated to 60 °C using a hot plate. During the heating process, the shape change of each section is recorded. Initially, both sections are at 0% transition with the manually set shape. When the temperature is above their thresholds, the SMA wires become straight, which leads to a 100% shape transition. Section 1 has a threshold of around 30 °C, and section 2 has a threshold of around 50 °C. In Figure 3, the measured temperature response of Section 1 is depicted as the blue dash line. Its shape starts to change at 28 °C and finishes changing at 32 °C, resulting in a 4 °C transition zone. Similarly, the measured response of section 2, shown as the solid red line, starts to change shape at 48 °C drastically and finishes changing at 53 °C. The transition zone is 5 °C.

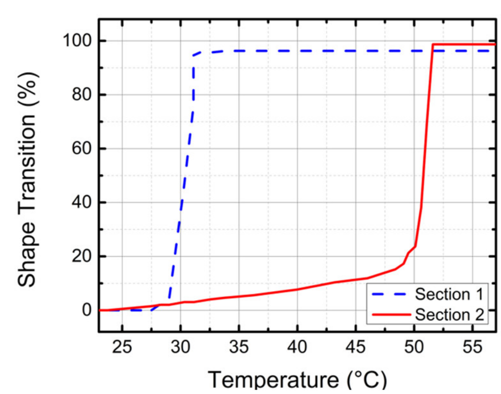


*Figure 3: Temperature response of the SMA.*

**Frequency Response vs. Temperature**

The $S_{11}$ of the actual fabricated SMA antenna at different temperatures is characterized by a Vector Network Analyzer (Agilent N5227A). The frequency responses of the SMA antennas are tested under three temperature ranges, which is below 30 °C, between 30 °C and 50 °C, and above 50 °C. The figures of the SMA antennas under different states are shown in Figure 4.

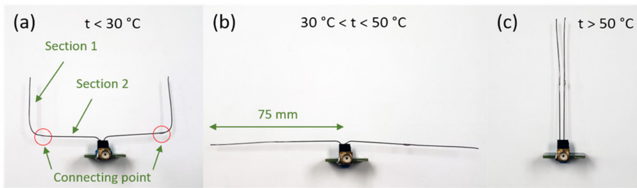


*Figure 4: Return loss configured SMA antenna under (a) no temperature violation, t < 30 °C, (b) first degree of temperature violation, 30 °C < t < 50 °C, and (c) second degree of temperature violation, t > 50 °C.*

The measured frequency response of the SMA antenna is shown in Figure 5. The return loss configuration is in a U shape state when the temperature is below 30 °C, as shown in Figure 4(a). Similar to the simulation results, the antenna in this state shows the most significant reflection of 30 dB at 950 MHz. When the temperature is between 30 °C and 50 °C, the SMA sensor transforms into a dipole antenna, as shown in Figure 4(b). As a result, the reflection coefficient $S_{11}$ drops to 24 dB at 950 MHz. As the temperature rises above 50 °C, the SMA antenna turns into a parallel antenna, as shown in Figure 4(c), and the $S_{11}$ is less than 3 dB over the 0.7 GHz to 1.2 GHz frequency range.

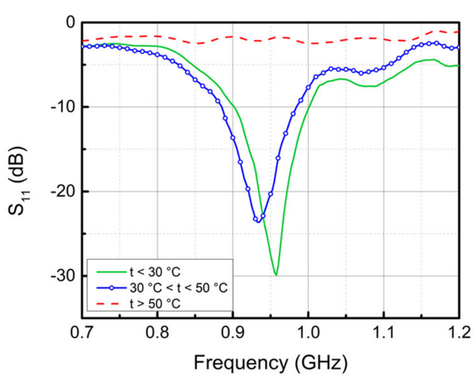


*Figure 5: Measured frequency response of the SMA antenna.*

## DISCUSSION

The SMA antenna presents a transition zone during the sweep of temperature, and the transition is not abrupt. The fabricated multi-section SMA wire will react to two different temperature thresholds. As indicated in Figure 4, the first section will change from the manually set shape to a predefined shape due to the SMA's thermal-mechanical memory effect. The transition-start temperature $A_s$ is 28 °C, and the transition-finish temperature $A_f$ is 32 °C. The 4 °C transition zone indicates a ±2 °C error for the first section at 30 °C. The second section has a higher threshold. Its transition-start temperature is 48 °C, and the transition-finish temperature is 53 °C. The tolerance for the second section is ±3 °C. Such a level of accuracy is suitable for temperature crossing monitoring for routine food and medical-grade products, where the goal is to provide some assurance, and accuracy of temperature sensing is not essential. To achieve more minor transition errors, one needs SMA wires with more rapid change, which can be fabricated by specific techniques and proper material selection [31,32,33]. However, this is not the focus of this paper.

For the proposed multi-section SMA antenna, the radiation response reveals the temperature range that the SMA antenna has experienced. Both simulation and experimental measurement justify that the temperature violation induced shape-change effect can be monitored by the magnitude of the reflection coefficient $S_{11}$ of the antenna. The return loss will be 30 dB when the temperature is below 30 °C. If the temperature ever rises between 30 °C and 50 °C, a 24 dB peak will be detected at 890 MHz in the $S_{11}$. If the highest temperature the antenna has experienced is above 50 °C, the return loss almost becomes a flat line over the frequency range. Due to the thermal-mechanical memory effect of the SMA wire, any temperature violation will cause the shape of the antenna to change, and the shape is kept (recorded) even after the temperature drops below the thresholds.

## CONCLUSION

In this work, a battery-free multi-section SMA-based antenna is presented to monitor dual temperature crossing events. Utilizing the thermo-mechanical memory effect of the SMA wire, the antenna changes its shape in accordance with the phase transition temperatures of the sections of SMA used to make the antenna. The shape change is maintained (recorded) even after the clearance of the temperature crossing event, achieving natural recording of event activity in the shape of the antenna. The return loss of the antenna is used as an electronic indicator of temperature crossing events. The significance of this sensor is that it offers battery-less multiple temperature thresholds sensing and recording, without the need for peripheral electronic components or batter, which provides a low-cost, and logistically easy to use solution for monitoring temperature-sensitive goods.

## REFERENCES

[1] P. Sen, S. N. R. Kantareddy, R. Bhattacharyya, S. E. Sarma, and J. E. Siegel, "Low-cost diaper wetness detection using hydrogel-based RFID tags", in IEEE Sensors Journal, 20(6), 3293(2020).

[2] X. Chen, H. He, Z. Khan, L. Sydänheimo, L. Ukkonen, and J. Virkki, "Textile-based batteryless moisture sensor", in IEEE Antennas and Wireless Propagation Letters, 19(1), 198(2020).

[3] V. Vivekananthan, N. R. Alluri, Y. Purusothaman, A. Chandrasekhar, S. Selvarajan, and S.-J. Kim, "Biocompatible collagen nanofibrils: an approach for sustainable energy harvesting and battery-free humidity sensor applications", ACS Appl. Mater. Interfaces, 10, 18650(2018).

[4] H. Guo, J. Chen, L. Tian, Q. Leng, Y. Xi, and C. Hu, "Airflow-induced triboelectric nanogenerator as a self-powered sensor for detecting humidity and airflow rate", ACS Appl. Mater. Interfaces, 6, 17184(2014).

[5] F. Pereira, R. Correia, M. Jordão and N. B. Carvalho, "Chipless strain sensor using phase modulation", 2020 IEEE Wireless Power Transfer Conference (WPTC), 420(2020).

[6] A. Mehmood et al., "Body movement-based controlling through passive RFID integrated into clothing", in IEEE Journal of Radio Frequency Identification, 4(4), 414(2020).

[7] W. Wang, R. Owyeung, Sadeqi, A. Sadeqi, and S. Sonkusale, "Single event recording of temperature and tilt using liquid metal with RFID tags", IEEE Sensor Journal, 20(6), 3249(2020).

[8] Z. Qian, S. Kang, V. Rajaram, et al. "Zero-power infrared digitizers based on plasmonically enhanced micromechanical photoswitches", Nature Nanotech, 12, 969(2017).

[9] B. Rahmadya, X. Chen, S. Takeda, K. Kagoshima, M. Umehira

and W. Kurosaki, “Measurement of a UHF RFID-based battery-less vibration frequency sensitive sensor tag using tilt/vibration switches”, in IEEE Sensors Journal, 20(17), 9901(2020).
[10] W. Wang, A. Sadeqi, and S. Sonkusale, “All-around package security using radio frequency identification threads”, IEEE Sensor, 1(2018).
[11] W. Wang, A. Sadeqi, H. R. Nejad and S. Sonkusale, “Cost-Effective Wireless Sensors for Detection of Package Opening and Tampering”, IEEE Access, 8, 117122(2020).
[12] L. Zhu, N. Alsaab, M. M. -C. Cheng and P. -Y. Chen, “A zero-power ubiquitous wireless liquid-level sensor based on microfluidic-integrated microstrip antenna”, in IEEE Journal of Radio Frequency Identification, 4(3), 265(2020).
[13] K. Bouzaffour, B. Lescop, P. Talbot, F. Gallée and S. Rioual, “Development of an Embedded UHF-RFID Corrosion Sensor for Monitoring Corrosion of Steel in Concrete”, in IEEE Sensors Journal, 21(10), 12306(2021).
[14] C. Asci, W. Wang and S. Sonkusale, “Security monitoring system using magnetically-activated RFID tags”, IEEE SENSORS, Rotterdam, Netherlands, 1(2020).
[15] W. Wang, C. Asci, and S. Sonkusale, “Security monitoring system uses RFID tags”, EDN, (2020), https://www.edn.com/security-monitoring-system-uses-rfid-tags/
[16] W. Wang, C. Asci, W.Zeng, and S. Sonkusale, “Zero-Power Screen Printed Flexible RFID Sensors for Smart Home Journal of Ambient Intelligence and Humanized Computing, in process.
[17] Cook, B.S.; Vyas, R.; Kim, S.; Thai, T.; Le, T.; Traille, A.; Aubert, H.; Tentzeris, M.M. “RFID-based sensors for zero-power autonomous wireless sensor networks”, IEEE Sens, 14, 2419(2014).
[18] Khalid, N.; Mirzavand, R.; Saghlatoon, H.; Honari, M.M.; Mousavi, P. “A three-port zero-power RFID sensor architecture for IoT applications”, IEEE Access, 8, 66888(2020).
[19] K. Biji, C. Ravishankar, C. Mohan, and T. Srinivasa Gopal, “Smart packaging systems for food applications: a review”, J. Food Sci. Technol, 52(10), 6125(2015).
[20] W. Wang, W. Zeng, and S. Sameer, “Tunable radiofrequency antenna using material programming”, unpublished.
[21] W. Wang, W. Zeng, and. Sonkusale, “Battery-free shape-memory alloy antennas for detection and recording of peak temperature activity”, Crystals, 12(1), 86(2022).
[22] W. Wang, C. Asci, W. Zeng, and S. Sonkusael, “Shape memory alloy-based helix antenna for temperature sensing”, unpublished.
[23] W. Wang, W. Zeng, A. Sadeqi, and S. Sonkusale, “Wireless temperature monitoring with shape memory alloy-based antenna”, IEEE Antennas and Wireless Propagation Letters, pp. 313-316, Jan. 2021.
[24] S. Jiang, Y. Zhang, Y. Zhao, “Dynamic recovery and dynamic recrystallization of NiTi shape memory alloy under hot compression deformation”, Transactions of Nonferrous Metals Society of China, 23(1), 140(2013).
[25] A. Nespoli, F. Passaretti, E. Villa, “Phase transition and mechanical damping properties: A DMTA study of NiTiCu shape memory alloys”, Intermetallics, 32, 394(2013).
[26] J. M. Jani, M. Leary, A. Subic, M. A. Gibson, “A review of shape memory alloy research, applications and opportunities”, Materials & Design (1980-2015), 56, 1078(2014).
[27] Y. Liu, J. V. Humbeeck, R. Stalmans, L. Delaey, “Some aspects of the properties of NiTi shape memory alloy”, Journal of Alloys and Compounds, 247(1–2),115(1997).
[28] W. Wang, W. Zeng, W. Ruan, E. Miller, and S. Sonkusale, “Thermo-mechanically trained shape memory alloy for temperature recording with visual readout”, IEEE Sensors Letters, 5, (1), 1(2021).
[29] R. Hahnlen, G. Fox, and M. Dapino, “Ultrasonic soldering of shape memory NiTi to aluminum 2024”, Supplement to the Welding Journal, 1(2012).
[30] N. W Pinto IV, N. L. Johnson, N. P. Irish, M. P. Balogh, D. B Haddad, “Method for soldering shape memory alloys”, U.S. Patent 14/931,056, issued September 26(2017).
[31] I. Mihálcz, “Fundamental characteristics and design method for nickel-titanium shape memory alloy”, Periodica Polytechnica Mechanical Engineering, 45(1), 75(2001).
[32] P. J. S. Buenconsejo, R. Zarnetta, D. König, A. Savan, S. Thienhaus, and A. Ludwig, “A new prototype two-phase (TiNi)–(β-W) SMA system with tailorable thermal hysteresis”, Adv. Funct. Mater., 21, 113(2011).
[33] J. Jiang, L. Cui, Y. Zheng, D. Jiang, Z. Liu, K. Zhao, “Narrow hysteresis behavior of TiNi shape memory alloy constrained by NbTi matrix during incomplete transformation”, Materials Science and Engineering: A, 536, 33(2012).

## CONTACT

*Sameer Sonkusale, tel: + 617-627-5113; sameer@ece.tufts.edu